Supplement of

ORCHIDEE MICT-LEAK (r5459), a global model for the production, transport and transformation of dissolved organic carbon from Arctic permafrost regions, Part 2: Model evaluation over the Lena River basin.

Authors:
S.P.K. Bowring[1], R. Lauerwald[2], B. Guenet[1], D. Zhu[1], M. Guimberteau[1,3], P. Regnier[2], A. Tootchi[3], A. Ducharne[3], P. Ciais[1]

Affiliations:
[1] Laboratoire des Sciences du Climat et de l'Environnement, LSCE, CEA, CNRS, UVSQ, 91191 Gif Sur Yvette, France
[2] Department of Geoscience, Environment & Society, Université Libre de Bruxelles, Bruxelles, Belgium
[3] Sorbonne Université, CNRS, EPHE, Milieux environnementaux, transferts et interaction dans les hydrosystèmes et les sols, Metis, 75005 Paris, France

Text S1: Groundwater DOC Concentrations

The high groundwater reservoir DOC concentrations simulated in high altitude regions by ORCHIDEE MICT-L is related to the fact that, in the model, DOC is rapidly produced and infiltrated deep into soil above the permafrost table, to the point that it reaches the simulated groundwater pool relatively quickly, allowing it to enter this reservoir before being metabolised through the soil column –hence allowing for the relatively high groundwater concentrations found in mountain areas. Because of the prevailing low temperatures, this DOC is not quickly decomposed by microbes and instead feed the groundwater DOC pool.

Text S2: Evaluation of Simulated NPP and Soil Respiration

Rates of yearly net primary production (NPP) for Russian and Siberian forests have been inferred in situ from eddy flux and inventory techniques to range from 123-250 gC m^{-2} yr^{-1} (Beer et al., 2006; Lloyd et al., 2002; Roser et al., 2002; Schulze et al., 1999; Shvidenko and Nilsson, 2003). We likewise simulate a broad range of NPP carbon uptake rates, of 61-469 gC m^{-2} yr^{-1} averaged per grid cell over the Lena basin, with a mean value of 210 gC m^{-2} yr^{-1}. NPP is heterogeneously distributed over space and between PFTs (SI, Fig. S5c), with forests averaging 90 gC m^{-2} yr^{-1} and grasslands averaging 104 gC m^{-2} yr^{-1} over the basin as a whole. Low values tended to originate in basin grid cells with elevated topography or high mean slope, while the maximum value was standalone, exceeding the next greatest by ~100 gC m^{-2} yr^{-1}, and is most likely caused by the edge effects of upscaling a coastal gridcell's small fraction of terrestrial area where high productivity occurs in a small plot, to the grid cell as a whole. By evaluating NPP we are also evaluating at a secondary level litter production, which is at a third level a major component of DOC production.

Taken as a whole, gross primary production (GPP) was performed under simulations by four PFT groups, with the largest basin-wide bulk contributions coming from boreal

needleleaf summer-green trees and C3 grasses (SI, Fig. S5a), the highest GPP uptake rates (3 TgC pixel^{-1} yr^{-1}) generated by boreal needleleaf evergreen trees, and the remainder of GPP contributed by Boreal broad-leaved summer-green trees (SI, Fig. S5a).

Soil respiration rates, of combined soil heterotroph and plant root respiration in our Control simulation, averaged 208 gC m^{-2} yr^{-1} (0.57 gC m^{-2} d^{-1}) over the Lena basin over the period 1990-2000, which is somewhat higher than those found by Elberling (2007) in tundra soils over Svalbard, of 103-176 gC m^{-2} yr^{-1} (0.28-0.48 gC m^{-2} d^{-1}). Sawamoto, et al. (2000) measured in situ summertime soil respiration over the central Lena basin and found rates of 1.6-34 gC m^{-2} d^{-1}, while Sommerkorn (2008) observed rates of 0.1-3.9 gC m^{-2} d^{-1} at higher latitudes, these appearing to vary with vegetation and fire history, water table depth and temperature. Mean heterotrophic respiration rates of 1.6 gC m^{-2} d^{-1} are simulated here during July and August, in the range 0.0.5-2.2 gC m^{-2} d^{-1} for each of the above PFT groups. The spatial distribution of, and difference in respiration rates between PFT groups largely mirrors those for NPP (SI Fig. S5c), with maximum rates of 1.4 gC m^2 d^{-1} over forested sites, versus a maximum of 2.2 gC m^2 d^{-1} over grassland/tundra sites (SI, Fig. S5b).

Aggregated over the basin, results show that increases over the course of the 20th Century were simulated for NPP, GPP, River Discharge, DOC, $CO_{2(aq.)}$, autotrophic and heterotrophic respiration and CO_2 evasion, with percentage changes in the last versus first decade of +25%, +27%, 38%, +73%, +60%, +30%, +33% and +63%, respectively. (Fig. S7). It thus appears that rising temperatures and CO_2 concentrations disproportionately favoured the metabolisation of carbon within the soil and its transport and mineralisation within the water column, fed by higher rates of primary production and litter formation as well as an accelerated hydrological cycle.

Table S1: Data type, name and sources of data files used to drive the model in the study simulations.

Data Type	Name	Source
Vegetation Map	ESA CCI Land Cover Map	(Bontemps et al., 2013)
Topographic Index	STN-30p	(Vorosmarty et al., 2000)
Stream flow direction	STN-30p	Vörösmarty et al., 2000
River surface area		(Lauerwald et al., 2015)
Soil texture class		(Reynolds et al., 1999)
Climatology	GSWP3 v0, 1 degree	http://hydro.iis.u-tokyo.ac.jp/GSWP3/
Potential floodplains	Multi-source global wetland maps	(Tootchi et al., 2019)
Poor soils	Harmonized World Soil Database map	(Nachtergaele, Freddy, Harrij van Velthuizen, Luc Verelst, N. H. Batjes, Koos Dijkshoorn, V. W. P. van Engelen, Guenther Fischer, Arwyn Jones, 2010)
Spinup Soil Carbon Stock	20ky ORCHIDEE-MICT soil carbon spinup	(Guimberteau et al., 2018)

Table S2: Literature sources for empirical evaluation of model output.

	Empirical Evaluation Sources
DOC Discharge	Cauwet and Sidorov (1996); Dolman et al. (2012); Holmes et al. (2012); Lara et al. (1998); Raymond et al. (2007); Semiletov et al. (2011); Kutscher et al. (2017).
Water Discharge	Ye et al. (2009); Lammers et al. (2001)
DOC concentration	Shvartsev (2008); Denfeld et al. (2013); Mann et al. (2015); Raymond et al. (2007); Semiletov et al. (2011); Arctic-GRO/PARTNERS (Holmes et al., 2012)
NPP	Beer et al. (2006); Lloyd et al. (2002); Roser et al. (2002); Schulze et al. (1999); Shvidenko and Nilsson, (2003)
Soil Respiration	Elberling (2007); Sawamoto et al. (2000); Sommerkorn (2008).
CO2 Evasion	Denfeld et al. (2013); Serikova et al. (2018).

Table S3: Observed versus simulated DOC discharge (1998-2007), where we compare the output of two separate climatological datasets used as input to the model (GSWP3 and ISIMIP 2b). Also shown are the simulated versus observed DOC discharge for the six largest Arctic rivers (the "Big Six") and for the Pan-Arctic as a whole.

	Simulated DOC to Ocean	Simulated DOC to Ocean	Observations (Holmes et al., 2012)
	GSWP3	**ISIMIP 2b**	**PARTNERS/Arctic-GRO**
Lena	3.16	4.14	5.68
Big 6		19.36	18.11
Pan-Arctic		32.06	34.04

(a)

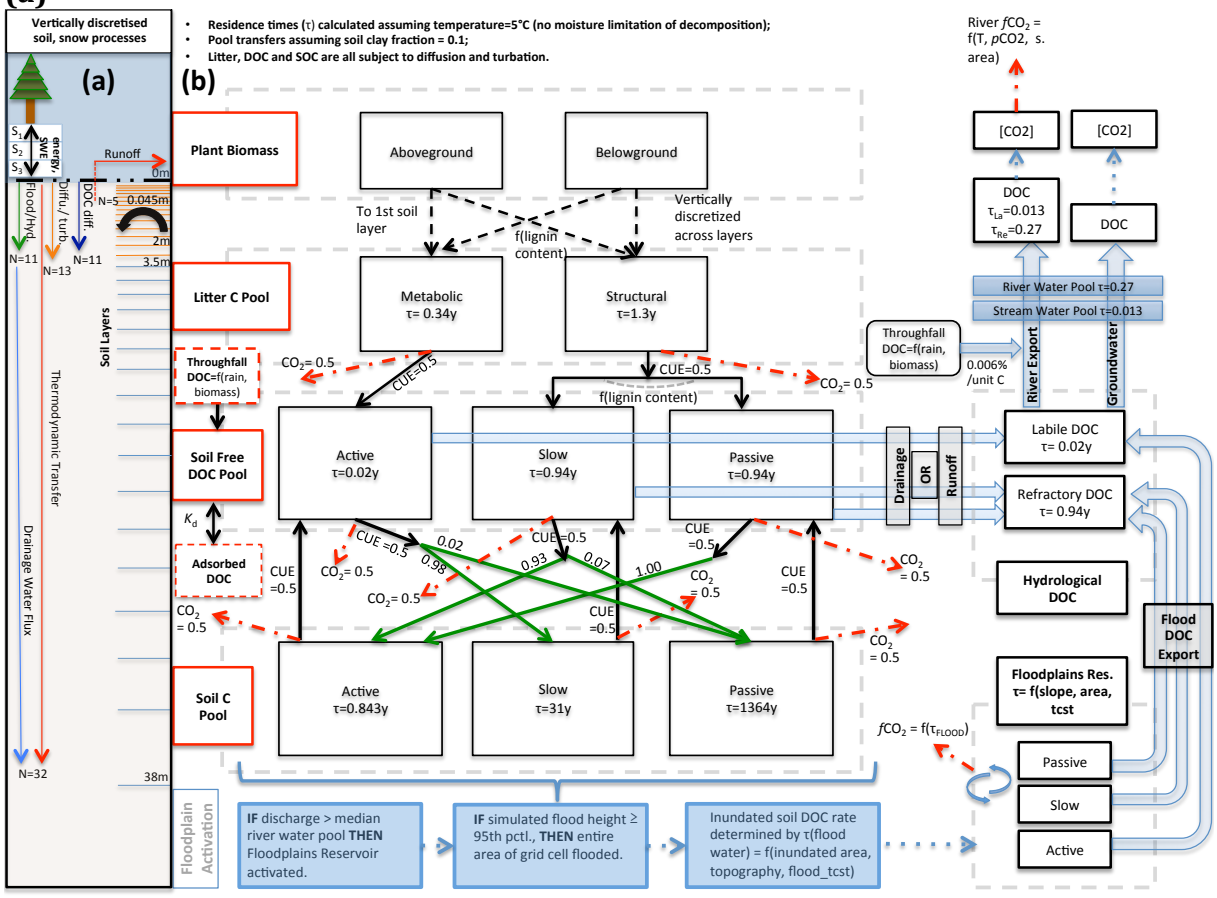

(c)

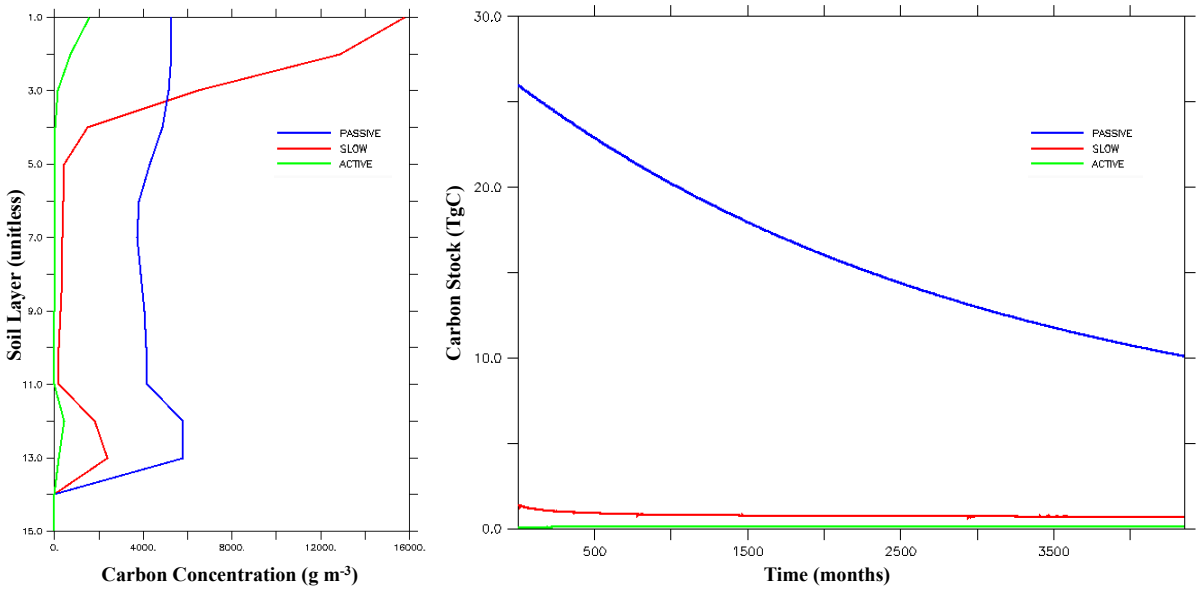

Figure S1: (a-b) Carbon and water flux map for core DOC elements in model structure relating to DOC transport and transformation, first published in Part 1 of this study. **(a)** Summary of the differing extent of vertical discretisation of soil and snow for different processes calculated in the model. Discretisation occurs along 32 layers whose thickness increases geometrically from 0-38m. N refers to the number of layers, SWE=snow water equivalent, S_n = Snow layer n. Orange layers indicate the depth to which diffusive carbon (turbation) fluxes occur. **(b)** Conceptual map of the production, transfer and transformation of carbon in its vertical and lateral (i.e., hydrological) flux as calculated in the model. Red boxes indicate meta-reservoirs of carbon, black boxes the actual pools as they exist in the model. Black arrows indicate carbon fluxes between pools, dashed red arrows give carbon loss as CO_2, green arrows highlight the fractional distribution of DOC to SOC (no carbon loss incurred in this transfer), a feature of this model. For a given temperature (5°C) and soil clay fraction, the fractional fluxes between pools are given for each flux, while residence times for each pool (τ) are in each box. The association of carbon dynamics with the hydrological module are shown by the blue arrows. Blue coloured boxes illustrate the statistical sequence which activates the boolean floodplains module. Note that for readability, the generation and lateral flux of dissolved CO_2 is omitted from this diagram, but is described at length in the Methods section. **(c)** (Left) Soil carbon concentrations per depth level for each soil carbon reactivity pool at the end of the spinup period. (Right) Evolution of each soil carbon pool over the course of the 400-year spinup quasi-eqliuibration period.

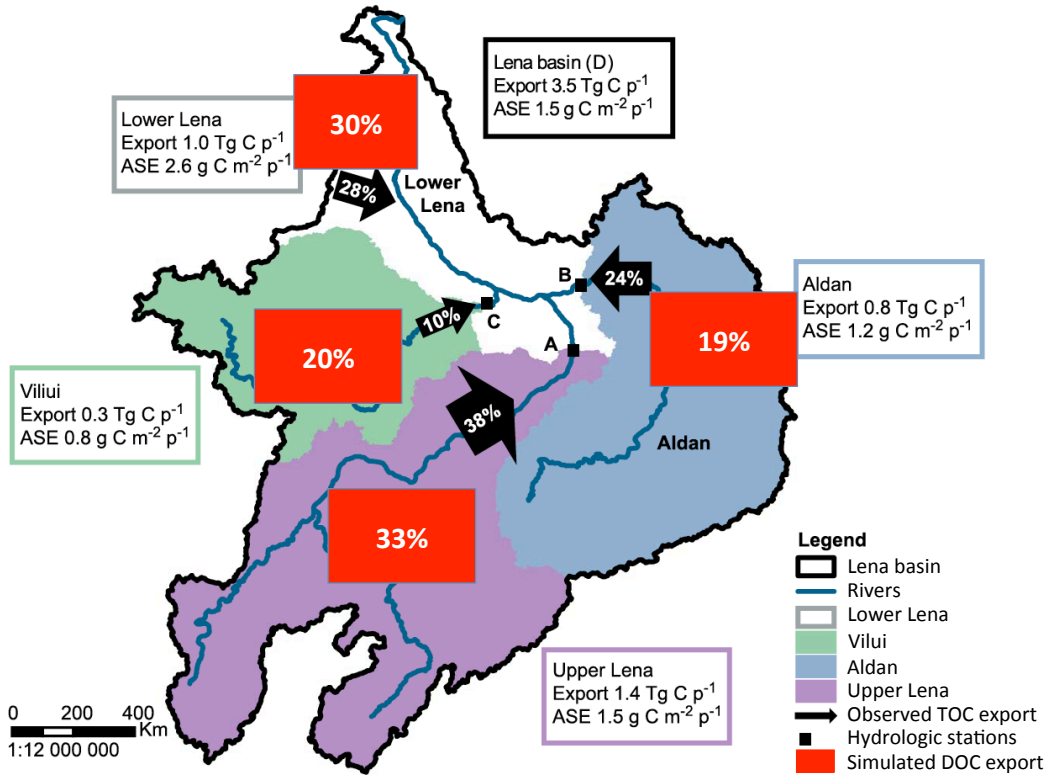

Figure S2: Map adapted from Fig. 2 in Kutscher et al. (2017) showing proportional sub-basin contributions of TOC outflow to total TOC discharge in June and July (designated as their sampling period 'p^{-1}') of 2012-2013, as observed in Kutscher et al., 2017 (black arrows), and DOC export contributions as simulated over the period 1998-2007 by ORCHIDEE MICT-L (red boxes). Simulation pixels used in the calculation are correlates of the real-world sampling locations unless the site coordinates deviated from a mainstem hydrographic flowpath pixel –in which case a nearest 'next-best' pixel was used. Here the percentages are out of the summed mean bulk DOC flow of each tributary, not the mean DOC discharge from the river mouth, because doing so would negate the in-stream loss of DOC via degradation to CO_2 while in-stream.

(a)

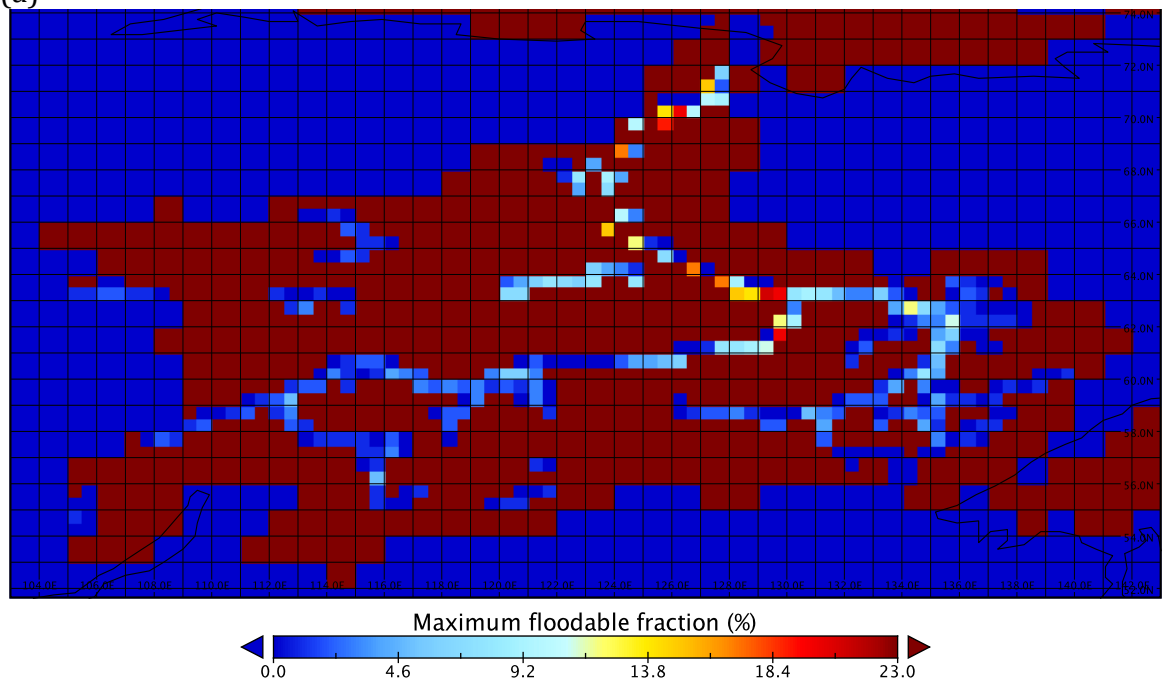

(b)

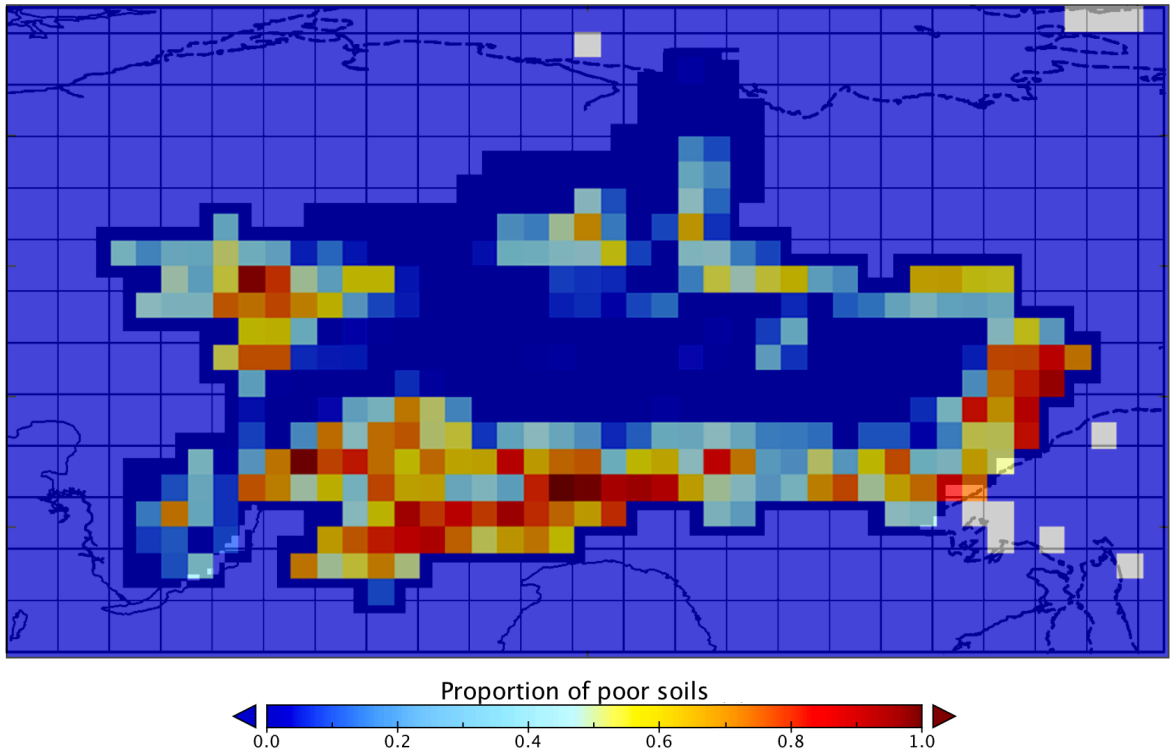

Figure S3: (a) Maximum floodable fraction of grid cells for the Lena basin per the input map from Tootchi et al. (2018). (b) Podzol and Arenosol map (Nachtergaele, Freddy, Harrij van Velthuizen, Luc Verelst, N. H. Batjes, Koos Dijkshoorn, V. W. P. van Engelen, Guenther Fischer, Arwyn Jones, 2010) used as input to the 'poor soils' module, basin mask in the background.

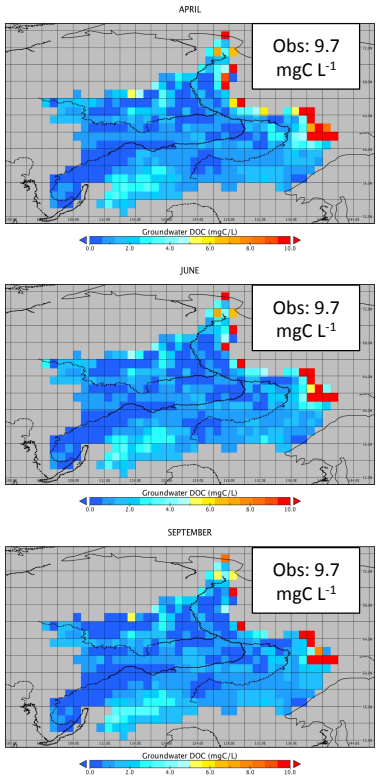

Figure S4: Groundwater DOC concentrations over the Lena basin for April, June and September averaged over 1998-2007, with mean observed concentrations for permafrost groundwater inset.

(a)

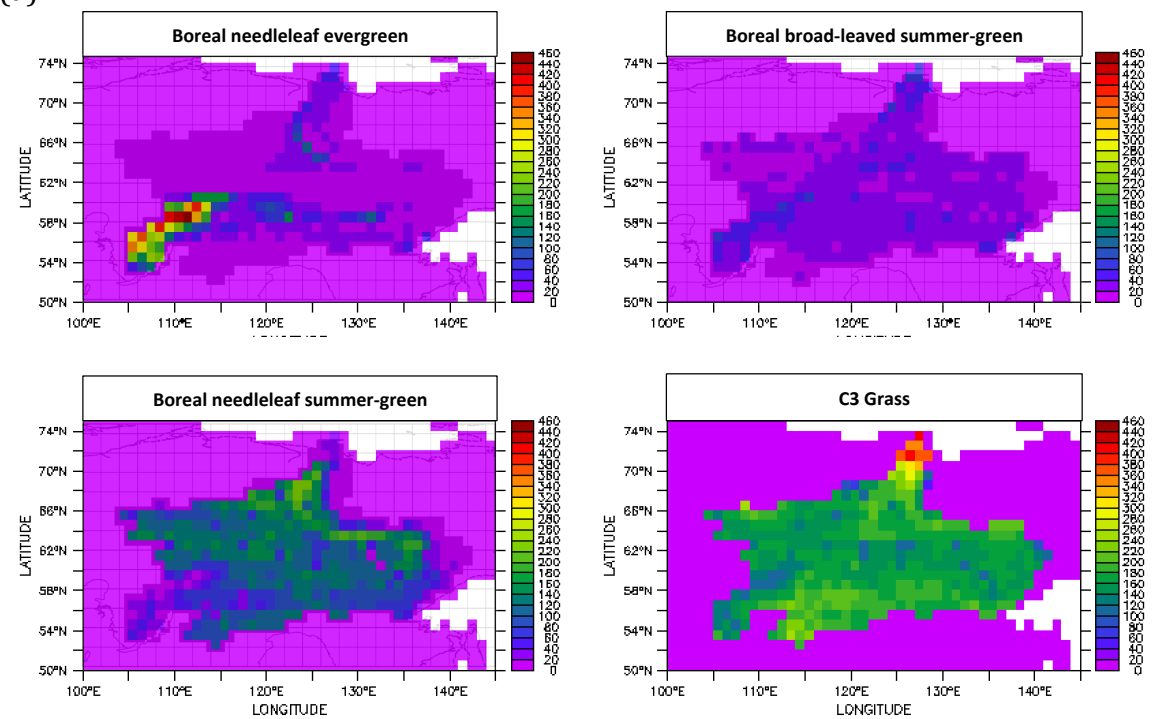

(b)

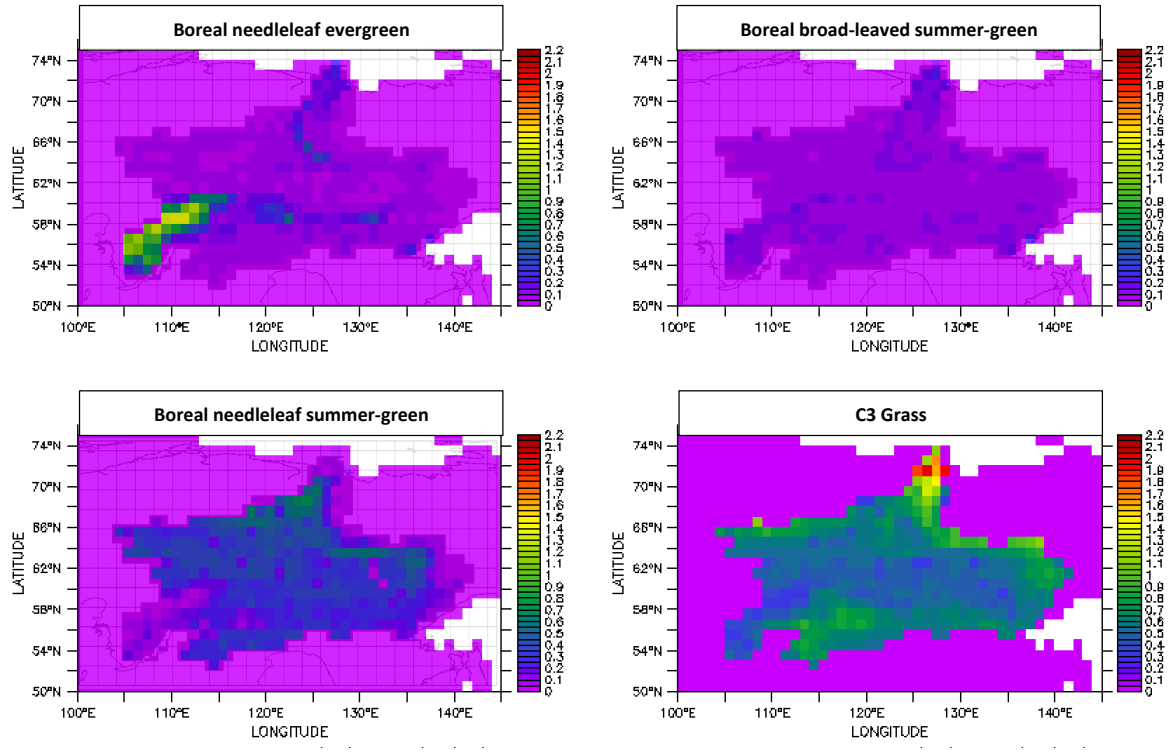
Boreal needleleaf evergreen
Boreal broad-leaved summer-green
Boreal needleleaf summer-green
C3 Grass
LATITUDE
LONGITUDE
74°N
70°N
66°N
62°N
58°N
54°N
50°N
100°E
110°E
120°E
130°E
140°E

(c)

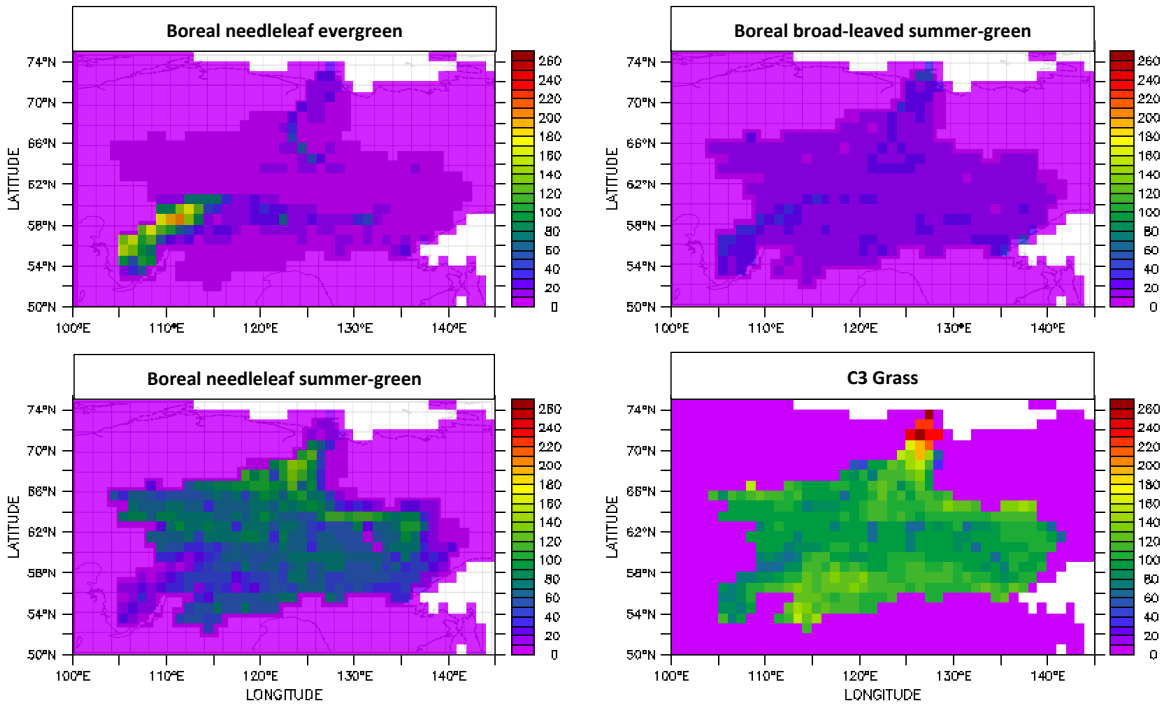
Boreal needleleaf evergreen
Boreal broad-leaved summer-green
Boreal needleleaf summer-green
C3 Grass
LATITUDE
LONGITUDE
74°N
70°N
66°N
62°N
58°N
54°N
50°N
100°E
110°E
120°E
130°E
140°E

(d)

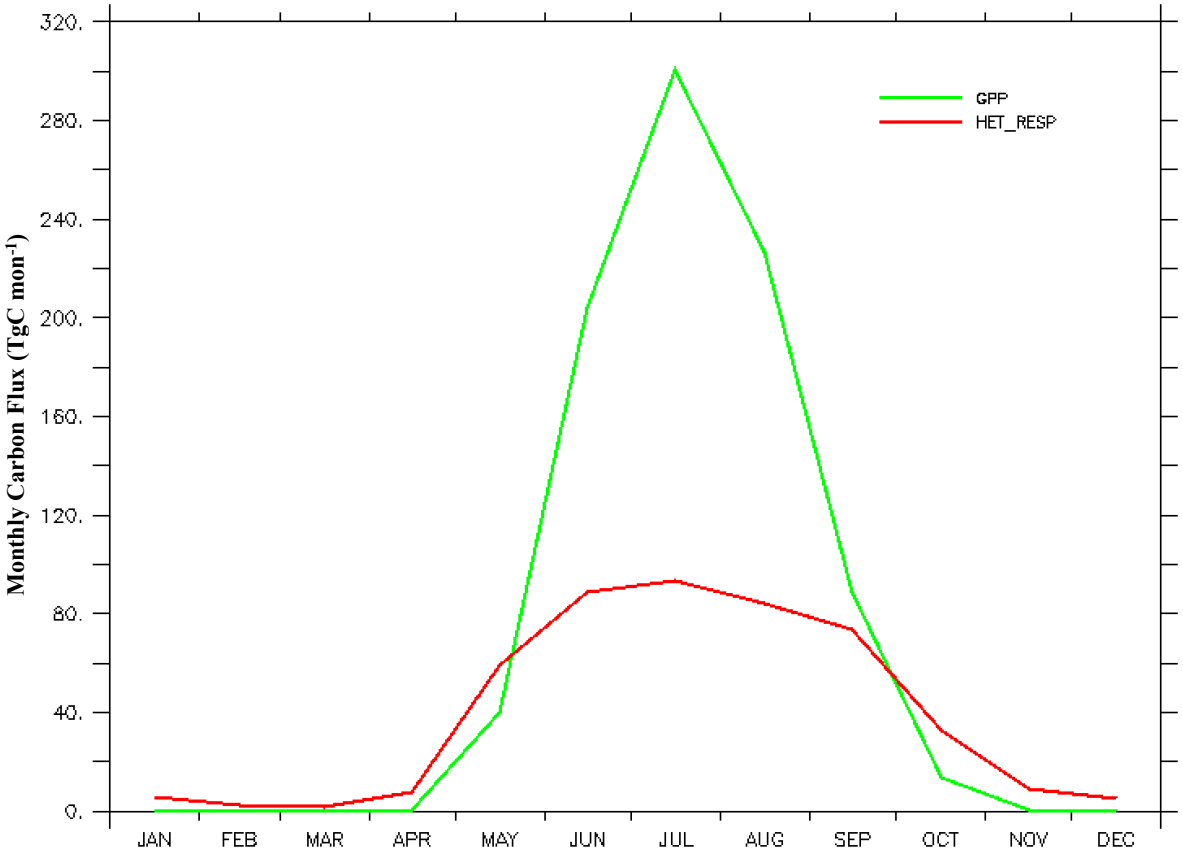

158
159 **Figure S5**: (a) Absolute yearly gross primary productivity (GPP, TgC yr^{-1}) for the four
160 relevant PFT groups over the Lena basin, averaged over 1998-2007. (b) Mean July and
161 August soil heterotrophic respiration rates (g m^2 d^{-1}) for the same PFT groups as in (a),
162 during the period 1998-2007. (c) Average yearly NPP (gC m^2 yr^{-1}) averaged over the
163 period 1998-2007. All maps have the Lena basin area shaded in the background. (d)
164 Mean monthly carbon uptake (GPP) versus its heterotrophic respiration from the soil
165 (Het_Resp) in TgC per month, over the period 1998-2007.
166

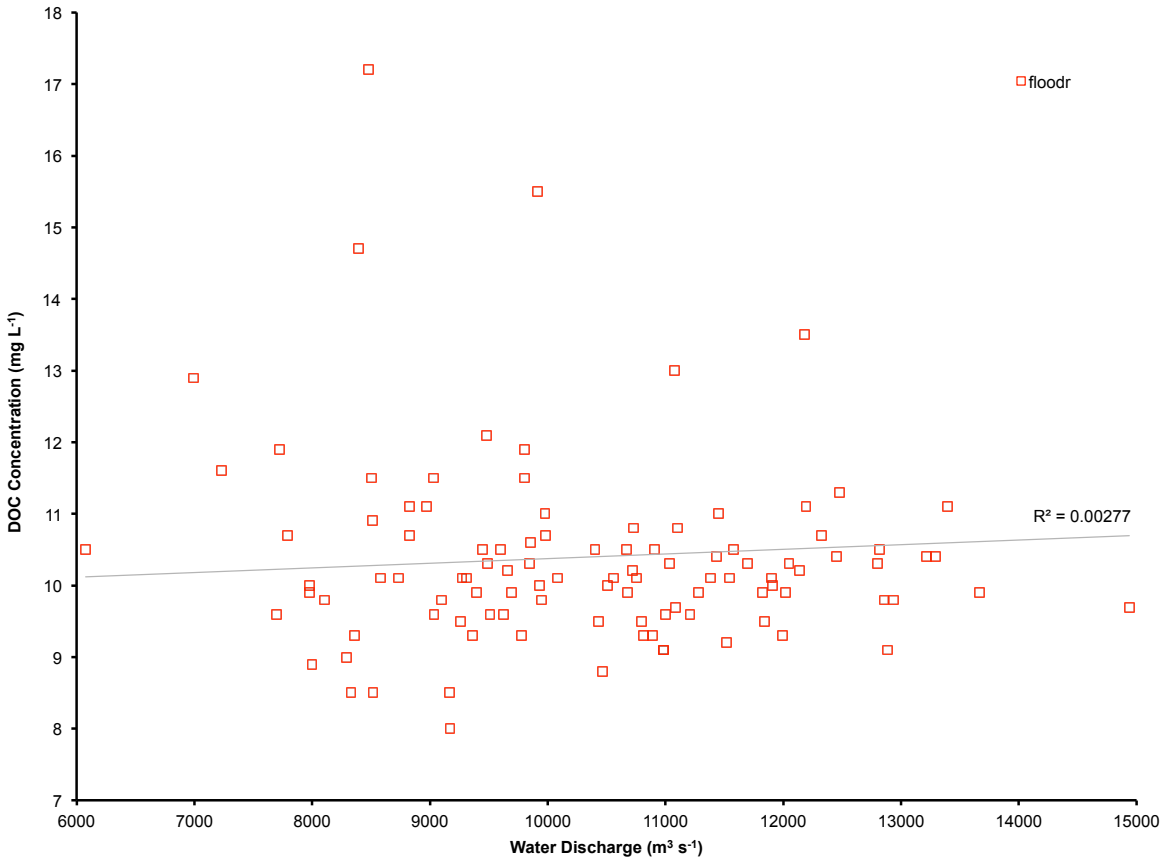

Figure S6: Simulated basin-mean annual DOC concentrations (mg L^{-1}) for the floodplain water pool regressed against mean annual simulated discharge rates at Kusur (m^3 s^{-1}) over 1901-2007. A linear regression with R^2 is plotted.

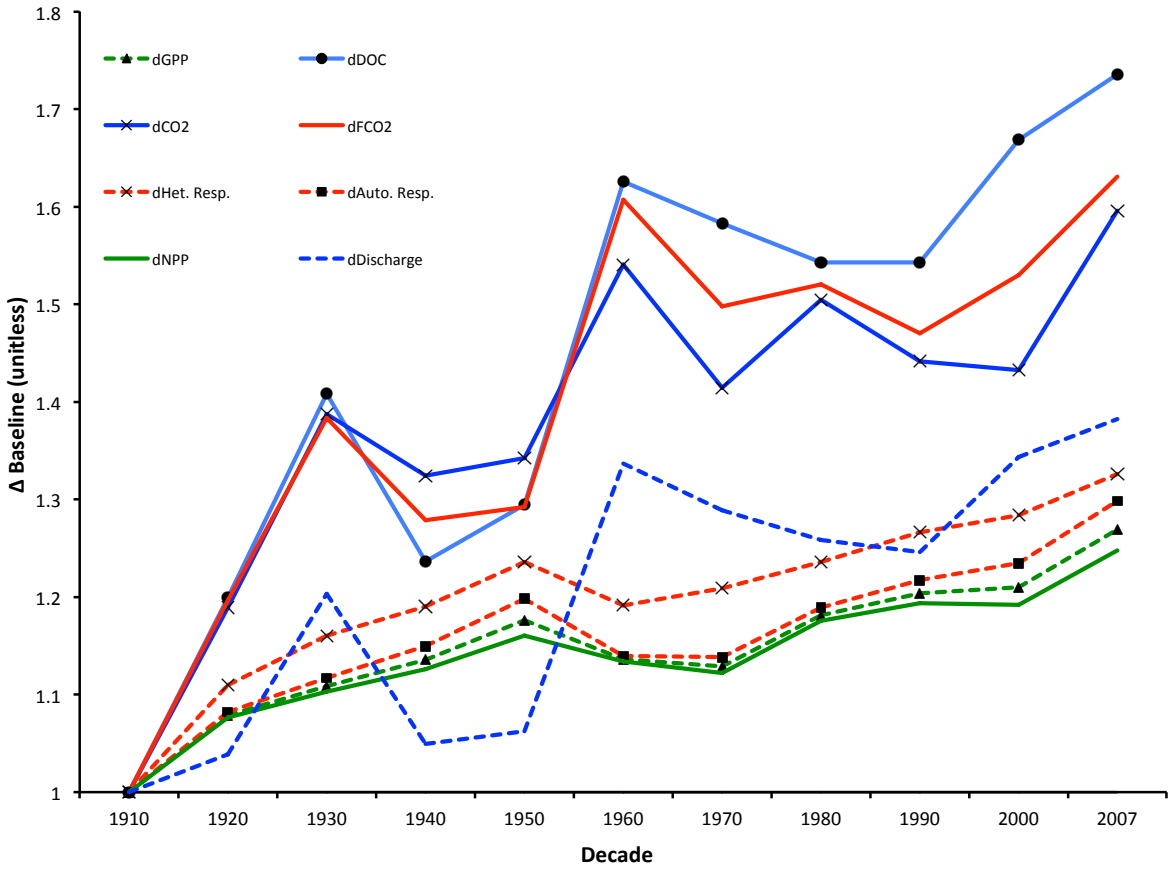

Figure S7: Time series showing the decadal-mean fractional change in carbon fluxes normalised to a 1901-1910 average baseline (=1 on the y-axis) for NPP, GPP, autotrophic and heterotrophic respiration, DOC inputs to the water column, CO_2 inputs to the water column, CO_2 evasion from the water surface (FCO2), and discharge.

References

Beer, C., Lucht, W., Schmullius, C. and Shvidenko, A.: Small net carbon dioxide uptake by Russian forests during 1981-1999, Geophys. Res. Lett., doi:10.1029/2006GL026919, 2006.

Bontemps, S., Defourny, P., Radoux, J., Van Bogaert, E., Lamarche, C., Achard, F., Mayaux, P., Boettcher, M., Brockmann, C., Kirches, G., Zülkhe, M., Kalogirou, V., Seifert, F. . and Arino, O.: Consistent global land cover maps for climate modelling communities: current achievements of the ESA' and cover CCI, in ESA Living Planet Symposium 2013, pp. 9–13., 2013.

Elberling, B.: Annual soil CO2effluxes in the High Arctic: The role of snow thickness and vegetation type, Soil Biol. Biochem., doi:10.1016/j.soilbio.2006.09.017, 2007.

Guimberteau, M., Zhu, D., Maignan, F., Huang, Y., Yue, C., Dantec-N d lec, S., Ottl, C., Jornet-Puig, A., Bastos, A., Laurent, P., Goll, D., Bowring, S., Chang, J., Guenet, B., Tifafi, M., Peng, S., Krinner, G., Ducharne, A. s., Wang, F., Wang, T., Wang, X., Wang, Y., Yin, Z., Lauerwald, R., Joetzjer, E., Qiu, C., Kim, H. and Ciais, P.: ORCHIDEE-MICT (v8.4.1), a land surface model for the high latitudes: model description and validation, Geosci. Model Dev., 11(1), 121–163, doi:10.5194/gmd-11-121-2018, 2018.

Lauerwald, R., Laruelle, G. G., Hartmann, J., Ciais, P. and Regnier, P. A. G.: Spatial patterns

in CO2evasion from the global river network, Global Biogeochem. Cycles, doi:10.1002/2014GB004941, 2015.
Lloyd, J., Shibistova, O., Zolotoukhine, D., Kolle, O., Arneth, A., Wirth, C., Styles, J. M., Tchebakova, N. M. and Schulze, E. D.: Seasonal and annual variations in the photosynthetic productivity and carbon balance of a central Siberian pine forest, Tellus, Ser. B Chem. Phys. Meteorol., doi:10.1034/j.1600-0889.2002.01487.x, 2002.
Nachtergaele, Freddy, Harrij van Velthuizen, Luc Verelst, N. H. Batjes, Koos Dijkshoorn, V. W. P. van Engelen, Guenther Fischer, Arwyn Jones, and L. M.: The harmonized world soil database, Proc. 19th World Congr. Soil Sci. Soil Solut. a Chang. World, Brisbane, Aust. 1-6 August 2010, pp. 34-37., 34–37 [online] Available from: https://library.wur.nl/WebQuery/wurpubs/fulltext/154132, 2010.
Reynolds, C. A., Jackson, T. J. and Rawls, W. J.: Estimating soil water-holding capacities by linking the Food and Agriculture Organization soil map of the world with global pedon databases and continuous pedotransfer functions, Water Resour. Res., 36(12), 3653–3662, doi:10.1029/2000WR900130, 1999.
Roser, C., Montagnani, L., Schulze, E.-D., Mollicone, D., Kolle, O., Meroni, M., Papale, D., Marchesini, L. B., Federici, S. and Valentini, R.: Net CO2 exchange rates in three different successional stages of the "Dark Taiga" of central Siberia, Tellus B, doi:10.1034/j.1600-0889.2002.01351.x, 2002.
Sawamoto, T., Hatano, R., Yajima, T., Takahashi, K. and Isaev, A. P.: Soil respiration in siberian taiga ecosystems with different histories of forest fire, Soil Sci. Plant Nutr., doi:10.1080/00380768.2000.10408759, 2000.
Schulze, E. D., Lloyd, J., Kelliher, F. M., Wirth, C., Rebmann, C., Luhker, B., Mund, M., Knohl, A., Milyukova, I. M., Schulze, W., Ziegler, W., Varlagin, A. B., Sogachev, A. F., Valentini, R., Dore, S., Grigoriev, S., Kolle, O., Panfyorov, M. I., Tchebakova, N. and Vygodskaya, N. N.: Productivity of forests in the eurosiberian boreal region and their potential to act as a carbon sink - a synthesis, Glob. Chang. Biol., doi:10.1046/j.1365-2486.1999.00266.x, 1999.
Shvidenko, A. and Nilsson, S.: A synthesis of the impact of Russian forests on the global carbon budget for 1961-1998, Tellus, Ser. B Chem. Phys. Meteorol., doi:10.1034/j.1600-0889.2003.00046.x, 2003.
Sommerkorn, M.: Micro-topographic patterns unravel controls of soil water and temperature on soil respiration in three Siberian tundra systems, Soil Biol. Biochem., doi:10.1016/j.soilbio.2008.03.002, 2008.
Tootchi, A., Jost, A. and Ducharne, A.: Multi-source global wetland maps combining surface water imagery and groundwater constraints, Earth Syst. Sci. Data, 11, 189–220, doi:10.5194/essd-11-189-2019, 2019.
Vorosmarty, C. J., Fekete, B. M., Meybeck, M. and Lammers, R. B.: Global system of rivers: Its role in organizing continental land mass and defining land-To-Ocean linkages, Global Biogeochem. Cycles, 14(2), 599–621, doi:10.1029/1999GB900092, 2000.